Neuro-adaptive hierarchical sliding mode control for a 3-wheeled mobile robot with disturbance rejection

Jose Carlos Vizarreta Mamani, Bladimir Leonel Vera Huamani, Raul Sulla Torres
Professional School of Electronic Engineering, Universidad Nacional de San Agustín de Arequipa, Arequipa, Peru

Article Info

ABSTRACT

High tracking accuracy and fast convergence are essential features in the control of wheeled mobile robots for autonomous navigation applications. However, the design of a control system for these robots faces significant challenges due to the inherent complexity of their nonlinear dynamics and their non-holonomic underactuated nature. This article introduces a novel control framework for trajectory tracking of a three-wheeled mobile robot (3WMR), considering external and internal disturbances. To address the uncertain nonlinear and underactuated non-holonomic dynamics of the 3WMR, an adaptive hierarchical fast terminal sliding mode control (AHFTSMC) strategy is proposed. In this approach, an adaptive neural network scheme adjusts the sliding surface coefficients in real time to minimize tracking errors and mitigate the chattering phenomenon. In addition, a finite time disturbance observer (FTDO) is designed to accurately estimate and compensate for unknown lumped disturbances, which helps to improve the disturbance rejection capability. The stability of the closed-loop system is demonstrated using Lyapunov theory. The proposed control approach is validated by numerical simulations, and a comparative analysis of recent hierarchical sliding mode controllers (SMC) is performed. The results demonstrate that the proposed approach achieves superior performance in terms of fast convergence and tracking accuracy, which are crucial features for the autonomous navigation of mobile robots.

Corresponding Author:

Jose Carlos Vizarreta Mamani
Professional School of Electronic Engineering, Universidad Nacional de San Agustín de Arequipa
Arequipa 04017, Perú
Email: jvizarretam@unsa.edu.pe

1. INTRODUCTION

In recent years, wheeled mobile robots have emerged as a significant field of research, driven by their agility and energy efficiency, which make them suitable for various applications such as logistics, security, and agriculture [1], [2]. Despite these advantages, controlling wheeled mobile robots presents significant challenges due to their nonlinear and complex dynamics, as well as their underactuated and non-holonomic nature, which means they possess more degrees of freedom than available control inputs [3]. Designing an autonomous control system for trajectory tracking in these robots is particularly challenging and requires advanced control techniques to ensure efficient performance.

Various control approaches have been investigated in the literature to tackle path tracking in wheeled mobile robots, including linear control techniques like proportional integral derivative (PID) [4], [5] and linear quadratic regulator (LQR) [6], [7]. For instance, [4] introduced a robust PID control structure enhanced by

genetic algorithms for better performance, while [5] proposed a double-loop fractional-order PID control to improve robustness and accuracy. Similarly, LQR control was applied in [6] using a cascade control scheme for a two-wheeled robot, and [7] combined PI and LQR controls to address trajectory tracking amidst obstacles. However, these linear control techniques present limitations in their effectiveness since they operate stably only near the equilibrium point, where the dynamic model of the system is linearized [8]. Moreover, they lack robustness in environments with large external and internal disturbances.

Given these limitations, nonlinear control techniques have gained relevance. Sliding mode control (SMC) is a popular nonlinear technique in robotics due to its robustness against uncertainties and ability to manage imprecise models [9], [10]. For example, second-order SMC was applied in [11], [12] for trajectory tracking of four-wheeled robots, incorporating adaptive laws in [11] and extended state observer in [12] to handle external disturbances. However, these approaches employ linear sliding surfaces that can cause chattering in the control signal, potentially damaging electric motors in practical applications [13].

Recently, control approaches with advanced sliding surfaces have been proposed to overcome these limitations and improve control performance in mobile robot trajectory tracking. For example, Labbadi *et al.* [14], a fractional-order SMC approach was designed for a differential mobile robotic system, while [15] proposed an adaptive non-singular fast terminal SMC scheme. However, these works [14], [15] did not take into account the full dynamic model of the mobile robot, limiting themselves only to kinematic control, and although they addressed external disturbances, they did not evaluate the robustness against internal disturbances. On the other hand, Goswami and Padhy [16], a dynamic controller based on a PID-type sliding surface was proposed for path tracking of a differentially driven mobile robot, taking into account measurement noise, frictional disturbances, and modeling inaccuracies. Xie *et al.* [17], a non-singular fast terminal SMC dynamic controller with adaptive laws to handle parametric uncertainties and external disturbances was presented. Finally, in the most recent work [18], an innovative PI-type adaptive SMC grounded in the dynamic model was presented for the path tracking of a mobile robot. Despite these advances, it is essential to note that these approaches [14]-[18] fail to achieve satisfactory tracking accuracy due to the underactuation problem inherent to non-holonomic wheeled mobile robots, which limits their ability to follow trajectories accurately.

Given the challenges associated with underactuated nonlinear systems, hierarchical sliding mode control (HSMC) has been investigated as a potential solution [19]. HSMC preserves the benefits of SMC while allowing simultaneous control of multiple outputs by decomposing the system into subsystems [20]. This approach has been broadly applied in the trajectory tracking of various underactuated systems, including inverted pendulums [21], aerial robots [22], flexible robotic manipulators [23], and wheeled mobile robots [24]-[27]. In the field of mobile robots, in [24], an HSMC with a PID-type sliding surface was proposed, showing promising results in tracking accuracy. However, the robustness of the control against external disturbances was not assessed. Wu and Karkoub [25], a hierarchical fuzzy sliding mode adaptive control (HFSMAC) with a PI-type sliding surface was presented, using fourier series-based function approximations to address uncertainties. More recent work [26], [27] combined backstepping and sliding mode techniques to develop a backstepping hierarchical sliding mode control (BHSMC). Although these approaches [24]-[27] improve trajectory tracking accuracy, it is essential to note that these works employed conventional sliding surfaces, which lead to asymptotic stability and hence slow convergence speed in time to the reference trajectory, limiting their applicability in practical environments where fast convergence in finite time is required.

The key findings from previous studies highlight the need for further research to address the unresolved issues in trajectory tracking control for wheeled mobile robots. Although the HSMC architecture has proven effective, there is a need for new control strategies with nonlinear sliding surfaces that can achieve high tracking accuracy, fast response, and robustness simultaneously. In this context, in this research, we propose a novel neuro-adaptive hierarchical SMC system for improved trajectory tracking in a three-wheeled mobile robot (3WMR). The main contributions of this paper are as follows: first, unlike previous works [24]-[27], which rely on conventional sliding surfaces, this research introduces an adaptive hierarchical fast terminal sliding mode control (AHFTSMC) strategy. Moreover, our method dynamically adjusts the sliding surface coefficients in real time through a neural network to reduce tracking errors and mitigate chattering effects. Second, a finite-time disturbance observer (FTDO) is developed to quickly and accurately estimate unknown lumped disturbances. Unlike previous approaches [24]-[27], this study considers external and internal disturbances affecting the mobile robot. Third, compared to existing control methods [25], [27], the proposed system demonstrates significantly superior performance in trajectory tracking, evidenced by faster convergence, higher accuracy, and enhanced robustness.

The remainder of the document is organized as follows: section 2 details the research methodology, which encompasses the dynamic modeling of the 3WMR, the development of the control system, and the stability evaluation. In section 3 provides the findings and analysis of the study. Lastly, section 4 offers the conclusions.

2. RESEARCH METHOD

This section presents the methodology adopted to address the trajectory tracking control problem of a 3WMR in the presence of external and internal disturbances. First, the mathematical modeling of the 3WMR is developed, which establishes the basis for the design and analysis of the control system. Next, the design of the proposed control system is introduced, consisting of three main components: a FTDO, a nonlinear control strategy, and adaptive laws based on a neural network. Finally, a stability analysis of the closed-loop system is conducted to ensure that the tracking errors converge to zero within a finite time.

2.1. Mathematical model

A 3WMR is a non-holonomic robotic system consisting of two driving wheels and a rotating wheel, allowing it to move horizontally. This mobile robot operates with differential drive, meaning the two rear wheels are powered, allowing the driving and steering functions to be controlled independently. Figure 1 shows a top view of the 3WMR in a horizontal plane, where (O_B, X_B, Y_B) represents the coordinate frame fixed on the mobile robot, and (O_G, X_G, Y_G) represents the global coordinates. The position vector of the mobile robot is denoted as $q = [x, y, \theta]^T$ where x and y represent the cartesian position, and θ represents the orientation.
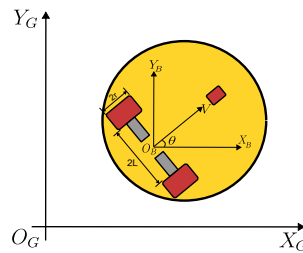

Figure 1. Non-holonomic 3WMR

Using the Euler-Lagrange formulation, the following equation describes the dynamics and kinematics of the non-holonomic 3WMR [3]:

$$M(q)\ddot{q} + C(q, \dot{q})\dot{q} = E(q)T - A^T(q)\lambda \tag{1}$$

here $M(q)$ represents a positive definite inertia matrix, $C(q, \dot{q})$ denotes the Coriolis matrix along with the centripetal terms, $A(q)$ is the matrix related to the nonholonomic constraints, T represents the vector of input, and $E(q)$ is the transformation matrix of the control inputs. Their expressions are denoted by [27].

$$M(q) = \begin{bmatrix} m & 0 & 0 \\ 0 & m & 0 \\ 0 & 0 & J \end{bmatrix}, C(q, \dot{q}) = \begin{bmatrix} 0 \\ 0 \\ 0 \end{bmatrix}, T = \begin{bmatrix} T_1 \\ T_2 \end{bmatrix}$$

$$E(q) = \frac{1}{r} \begin{bmatrix} cos\,\theta & cos\,\theta \\ sin\,\theta & sin\,\theta \\ L & -L \end{bmatrix}, A^T(q) = \frac{1}{r} \begin{bmatrix} -sin\,\theta \\ cos\,\theta \\ 0 \end{bmatrix} \tag{2}$$

The characteristics of the 3WMR are outlined as follows: m and J indicate the mass and moment of inertia of the mobil robot, respectively. T_1 and T_2 are the torques exerted by the right and left motors associated with the driving wheels. In addition, r is the radius of the driving wheels, L signifies half the distance between the rear wheels, and λ represents the Lagrange multiplier.

Taking into account non-holonomic constraints and conditions for anti-slip rolling, we derive the (3).

$$\dot{x}\,sin\,\theta - \dot{y}\,cos\,\theta = 0 \tag{3}$$

The determination of the Lagrangian bond strength factor is performed as (4) [26].

$$\lambda = -m\,\theta(\dot{x}\,cos\,\theta - \dot{y}\,sin\,\theta) \tag{4}$$

Therefore, the dynamic model of the 3WMR is described as (5) [27]:

$$\begin{cases} \ddot{x} = \dfrac{\lambda}{m}\,sin\,\theta + \dfrac{1}{r\,m}cos\,\theta\,u_1 + d_x(t), \\[2mm] \ddot{y} = -\dfrac{\lambda}{m}\,cos\,\theta + \dfrac{1}{r\,m}sin\,\theta\,u_1 + d_y(t), \\[2mm] \ddot{\theta} = \dfrac{L}{r\,J}\,u_2 + d_\theta(t), \end{cases} \tag{5}$$

where $u_1 = T_1 - T_2$, $u_2 = T_1 + T_2$ represent the control inputs, with $T_1 = 0.5(u_1 + u_2)$ and $T_2 = 0.5(u_2 - u_1)$. The terms $d_x(t), d_y(t), d_\theta(t)$ denote the unknown lumped disturbances affecting the mobile robot.

2.2. Proposed control system design

This section outlines the development of the proposed control system. Initially, the design of the FTDO, intended to estimate and mitigate the combined disturbances, is explained. Following this, the control approach is formulated. Based on the dynamic model in (5), the control framework is separated into underactuated and fully actuated components. The underactuated system is responsible for controlling the Cartesian position of the mobile robot, i.e., the variables x and y, with a single control action. To achieve this, an underactuated control architecture called the HFTSMC strategy is employed. Conversely, the fully actuated system is responsible for controlling the orientation of the mobile robot, for which the FTSMC strategy is employed. Finally, the adaptive laws are designed to adjust the sliding surface coefficients in real-time dynamically. Figure 2 illustrates the design of the proposed control system.
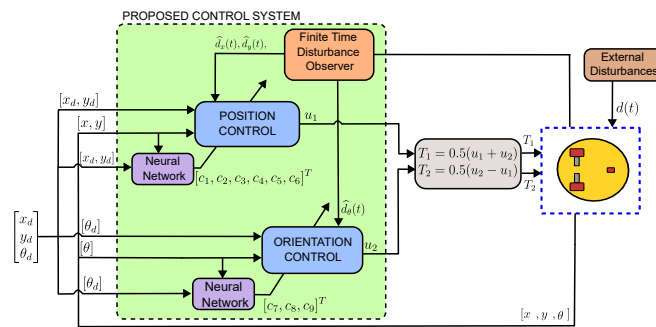

Figure 2. Proposed control system structure

2.2.1. FTDO design

In (5) can be expressed in the state space representation as:

$$\begin{aligned} \dot{\Pi}_{\mathcal{T}} &= \Pi_{\mathcal{T}+1} \\ \dot{\Pi}_{\mathcal{T}+1} &= f(\Pi_{\mathcal{T}}) + g(\Pi_{\mathcal{T}})u + d(t) \end{aligned} \tag{6}$$

here, $\Pi_{\mathcal{T}} = [x, \dot{x}, y, \dot{y}, \theta, \dot{\theta}]^T$ denotes the state vector, $u = [u_1, u_2]^T$ represents the control actions, $f(\Pi_{\mathcal{T}})$ and $g(\Pi_{\mathcal{T}})$ are two continuous functions that depend on $\Pi_{\mathcal{T}}$, and $d(t)$ indicates the aggregated disturbances.

- Assumption 1, the derivative of $d(t)$ is bounded and satisfies $\lim_{t\to\infty} \dot{d}(t) = 0$.
- Theorem 1 considering the dynamic system in (6), the FTDO design is defined as follows [8], [28]:

$$\dot{\Upsilon}_0 = \Gamma_0 + f(\Pi_{\mathcal{T}}) + g(\Pi_{\mathcal{T}})u$$
$$\Gamma_0 = -\xi_1 L_q^{1/3}|\Upsilon_0 - \dot{q}|^{2/3}\text{sign}(\Upsilon_0 - \dot{q}) + \Upsilon_1$$
$$\dot{\Upsilon}_1 = \Gamma_1 \tag{7}$$
$$\Gamma_1 = -\xi_2 L_q^{1/2}|\Upsilon_1 - \Gamma_0|^{1/2}\text{sign}(\Upsilon_1 - \Gamma_0) + \Upsilon_2$$
$$\dot{\Upsilon}_2 = -\xi_3 L_q \text{sign}(\Upsilon_2 - \Gamma_1)$$

where $\xi_i, i = \overline{1,2,3}$, and L_q are constant values defined as positive, which represent the gains of the observer. The variables Υ_0, Υ_1, and Υ_2 represent the estimates of $\dot{q}$, $d(t)$ and $\dot{d}(t)$, respectively, where $\dot{q} = [\dot{x}, \dot{y}, \dot{\theta}]^T$ denotes the velocity of the mobile robot. This configuration of FTDO can accurately identify the lumped disturbances $d(t)$ in finite time [28].

- Proof 1 we define observer errors as follows:

$$e_1^{obs} = \Upsilon_0 - \dot{q}, e_2^{obs} = \Upsilon_1 - d(t), e_3^{obs} = \Upsilon_2 - \dot{d}(t) \tag{8}$$

by performing the time derivative of (8) and substituting (7), the following expression is obtained:

$$\dot{e}_1^{obs} = -\xi_1 L_q^{1/3}|e_1^{obs}|^{2/3}\text{sign}(e_1^{obs}) + e_2^{obs}$$
$$\dot{e}_2^{obs} = -\xi_2 L_q^{1/2}|e_2^{obs} - \dot{e}_1^{obs}|^{1/2}\text{sign}(e_2^{obs} - \dot{e}_1^{obs}) + e_3^{obs} \tag{9}$$
$$\dot{e}_3^{obs} = -\xi_3 L_q \text{sign}(e_3^{obs} - \dot{e}_2^{obs}) - \ddot{d}(t)$$

the rest of the proof is similar to Theorem 1 of [8], so it is omitted for space reasons. Nevertheless, according to that theorem, the observation errors e_1^{obs}, e_2^{obs}, and e_3^{obs} converge to the origin in finite time by appropriately selecting the parameters ξ_1, ξ_2, ξ_3, and L_q, i.e. $\Upsilon_0 \equiv \widehat{\dot{q}}$, $\Upsilon_1 \equiv \widehat{d}(t)$, $\Upsilon_2 \equiv \widehat{\dot{d}}(t)$.

2.2.2. HFTSMC strategy design

Considering the dynamic model of the non-holonomic 3WMR given in (5), the following dynamic model for the position control system is introduced.

$$\begin{cases} \ddot{x} = \dfrac{\lambda}{m}\sin\theta + \dfrac{1}{r\,m}\cos\theta\,u_1 + d_x(t), \\ \ddot{y} = -\dfrac{\lambda}{m}\cos\theta + \dfrac{1}{r\,m}\sin\theta\,u_1 + d_y(t), \end{cases} \tag{10}$$

Based on the HSMC theory [20], the underactuated dynamic system given in (10) is decomposed into two subsystems for each state. To achieve this, we define the following state variables: $X = [\chi_1, \chi_2, \chi_3, \chi_4] = [x, \dot{x}, y, \dot{y}]^T$. The state-space representation of (10) can then be expressed as (11):

$$\begin{cases} \dot{\chi}_1 = \chi_2, \\ \dot{\chi}_2 = f_1(X) + g_1(X)u_1 + d_x(t) \\ \dot{\chi}_3 = \chi_4, \\ \dot{\chi}_4 = f_2(X) + g_2(X)u_1 + d_y(t) \end{cases} \tag{11}$$

where,

$$f_1(X) = \frac{\lambda}{m}\sin\theta, \quad g_1(X) = \frac{1}{r\,m}\cos\theta\, f_2(X) = -\frac{\lambda}{m}\cos\theta, \quad g_2(X) = \frac{1}{r\,m}\sin\theta \tag{12}$$

Considering (11), we define the position tracking errors as:

$$e_1^x = \chi_1 - x_d, e_2^x = \chi_2 - \dot{x}_d e_1^y = \chi_3 - y_d e_2^y = \chi_4 - \dot{y}_d \tag{13}$$

deriving in time (13), we obtain the dynamics of the errors as (14).

$$\begin{cases} \dot{e}_1^x = e_2^x, \\ \dot{e}_2^x = f_1(X) + g_1(X)u_1 + d_x(t) - \ddot{x}_d. \end{cases}; \begin{cases} \dot{e}_1^y = e_2^y, \\ \dot{e}_2^y = f_2(X) + g_2(X)u_1 + d_y(t) - \ddot{y}_d. \end{cases} \tag{14}$$

To ensure accurate performance and fast convergence in the underactuated control system, and unlike the approaches in [26], [27], in this research we propose a robust nonlinear fast terminal sliding surface for the first layer of the hierarchical structure, defined as:

$$
\begin{aligned}
\sigma_x &= e_2^x + c_1 e_1^x + c_2 |e_1^x|^{\alpha_x} \text{sign}(e_1^x) + c_3 |e_1^x|^{\beta_x} \text{sign}(e_1^x) \\
\sigma_y &= e_2^y + c_4 e_1^y + c_5 |e_1^y|^{\alpha_y} \text{sign}(e_1^y) + c_6 |e_1^y|^{\beta_y} \text{sign}(e_1^y)
\end{aligned}
\tag{15}
$$

where $\alpha_i \geq 1$ and $0 < \beta_i < 1$ with $i = \overline{x,y}$. The parameters $c_i > 0,\ i = \overline{1,6}$, are the positive coefficients of the sliding surface, which will be adjusted using a neural network in the following section.

Deriving in time the sliding surfaces (15) and substituting the expressions (14), we obtain:

$$
\begin{aligned}
\dot{\sigma}_x &= \dot{e}_2^x + c_1 \dot{e}_1^x + c_2 \alpha_x |e_1^x|^{\alpha_x - 1} + c_3 \beta_x |e_1^x|^{\beta_x - 1} \\
&= f_1(X) + g_1(X)u_1 + d_x(t) - \ddot{x}_d + c_1 \dot{e}_1^x + c_2 \alpha_x |e_1^x|^{\alpha_x - 1} + c_3 \beta_x |e_1^x|^{\beta_x - 1} \\
\dot{\sigma}_y &= \dot{e}_2^y + c_4 \dot{e}_1^y + c_5 \alpha_y |e_1^y|^{\alpha_y - 1} + c_6 \beta_y |e_1^y|^{\beta_y - 1} \\
&= f_2(X) + g_2(X)u_1 + d_y(t) - \ddot{y}_d + c_4 \dot{e}_1^y + c_5 \alpha_y |e_1^y|^{\alpha_y - 1} + c_6 \beta_y |e_1^y|^{\beta_y - 1}
\end{aligned}
\tag{16}
$$

By setting $\dot{\sigma}_i = 0,\ i = \overline{x,y}$, we obtain the equivalent control laws for each subsystem:

$$
\begin{aligned}
u_{eq}^x &= \frac{1}{g_1(X)} \left[\ddot{x}_d - f_1(X) - \widehat{d}_x - c_1 \dot{e}_1^x - c_2 \alpha_x |e_1^x|^{\alpha_x - 1} - c_3 \beta_x |e_1^x|^{\beta_x - 1} - k_x \text{sign}(\sigma_x) \right] \\
u_{eq}^y &= \frac{1}{g_2(X)} \left[\ddot{y}_d - f_2(X) - \widehat{d}_y - c_4 \dot{e}_1^y - c_5 \alpha_y |e_1^y|^{\alpha_y - 1} - c_6 \beta_y |e_1^y|^{\beta_y - 1} - k_y \text{sign}(\sigma_y) \right]
\end{aligned}
\tag{17}
$$

where $k_x,\ k_y$ are the positive coefficients and will be adjusted using a neural network in the following section. The hierarchical total control law for the position control system can be expressed as follows [19]:

$$
u_1 = u_{eq}^x + u_{eq}^y + u_{sw}^{x,y}
\tag{18}
$$

where u_{eq}^x, u_{eq}^y are the equivalent control laws of the first layer of the hierarchical structure, and $u_{sw}^{x,y}$ is the switching control law.

Since we have already established the two sliding surfaces of the first layer according to (15), we proceed to define the sliding surface of the second layer of the hierarchical structure as follows:

$$
s_1 = \eta_1 \sigma_x + \eta_2 \sigma_y
\tag{19}
$$

where η_1 and η_2 are two positive definite design parameters. Deriving in time (19) and substituting the expressions of (16), we obtain:

$$
\begin{aligned}
\dot{s}_1 = \eta_1 \dot{\sigma}_x + \eta_2 \dot{\sigma}_y =\ &\eta_1 \left[f_1(X) + g_1(X)u_1 + \widehat{d}_x - \ddot{x}_d + c_1 \dot{e}_1^x + c_2 \alpha_x |e_1^x|^{\alpha_x - 1} + c_3 \beta_x |e_1^x|^{\beta_x - 1} \right] + \\
&\eta_2 \left[f_2(X) + g_2(X)u_1 + \widehat{d}_y - \ddot{y}_d + c_4 \dot{e}_1^y + c_5 \alpha_y |e_1^y|^{\alpha_y - 1} + c_6 \beta_y |e_1^y|^{\beta_y - 1} \right]
\end{aligned}
\tag{20}
$$

Substituting the expressions of (18) into (20) and performing some mathematical operations, we obtain the following expression:

$$
\begin{aligned}
\dot{s}_1 =\ &\eta_1 \left[f_1(X) + g_1(X)(u_{eq}^x + u_{eq}^y + u_{sw}^{x,y}) + \widehat{d}_x - \ddot{x}_d + c_1 \dot{e}_1^x + c_2 \alpha_x |e_1^x|^{\alpha_x - 1} + c_3 \beta_x |e_1^x|^{\beta_x - 1} \right] + \\
&\eta_2 \left[f_2(X) + g_2(X)(u_{eq}^x + u_{eq}^y + u_{sw}^{x,y}) + \widehat{d}_y - \ddot{y}_d + c_4 \dot{e}_1^y + c_5 \alpha_y |e_1^y|^{\alpha_y - 1} + c_6 \beta_y |e_1^y|^{\beta_y - 1} \right] \\
=\ &\eta_1 \left[g_1(X)(u_{eq}^y + u_{sw}^{x,y}) \right] + \eta_2 \left[g_2(X)(u_{eq}^x + u_{sw}^{x,y}) \right]
\end{aligned}
\tag{21}
$$

To ensure a fast reach to the sliding manifold, we use the exponential approach law, defined as:

$$
\dot{s}_1 = -k_1^{s_1} s_1 - k_2^{s_1} \text{sign}(s_1)
\tag{22}
$$

where $k_1^{s_1}$ and $k_2^{s_1}$ are two positive definite parameters. Therefore, combining expressions (21) and (22), we design the switching control law as:

$$
u_{sw}^{x,y} = \frac{1}{\eta_1 g_1(X) + \eta_2 g_2(X)} \left[-\eta_1 g_1(X)u_{eq}^y - \eta_2 g_2(X)u_{eq}^x - k_1^{s_1} s_1 - k_2^{s_1} \text{sign}(s_1) \right]
\tag{23}
$$

Finally, by substituting expressions (17) and (23) into (18), we obtain the final position control law of the mobile robot:

$$
u_1 = \frac{1}{\eta_1 g_1(X) + \eta_2 g_2(X)} \left[\eta_1 g_1(X)u_{eq}^x + \eta_2 g_2(X)u_{eq}^y - k_1^{s_1} s_1 - k_2^{s_1} \text{sign}(s_1) \right]
\tag{24}
$$

2.2.3. FTSMC strategy design

Considering the dynamic model of the non-holonomic 3WMR given in (5), the following dynamic model for the orientation control system is introduced:

$$\ddot{\theta} = \frac{L}{r\,J}\,u_2 + d_\theta(t) \tag{25}$$

The following state variables $X = [\chi_5, \chi_6] = [\theta, \dot{\theta}]^T$ are defined. Then, the state-space representation of (25) is given as:

$$\begin{cases} \dot{x_5} = x_6, \\ \dot{x_6} = g(\theta)u_2 + d_\theta(t) \end{cases}; g(\theta) = \frac{L}{r\,J} \tag{26}$$

considering (26), we define the tracking errors as:

$$e_1^\theta = \chi_5 - \theta_d, \quad e_2^\theta = \chi_6 - \dot{\theta}_d \tag{27}$$

deriving in time (35), we obtain the dynamics of the errors as (28).

$$\begin{cases} \dot{e}_1^\theta = e_2^\theta, \\ \dot{e}_2^\theta = g(\theta)u_2 + d_\theta(t) - \ddot{\theta}_d \end{cases} \tag{28}$$

To ensure accurate performance and fast convergence in the fully actuated control system, we propose a robust nonlinear fast terminal sliding surface, defined as:

$$s_2 = e_2^\theta + c_7 e_1^\theta + c_8 |e_1^\theta|^{\alpha_\theta} \mathrm{sgn}(e_1^\theta) + c_9 |e_1^\theta|^{\beta_\theta} \mathrm{sgn}(e_1^\theta) \tag{29}$$

where $\alpha_\theta \geq 1$ and $0 < \beta_\theta < 1$. The parameters $c_i > 0, \; i = \overline{7,9}$ are the positive coefficients of the sliding surface, which will be adjusted using a neural network in the following section.

Deriving in time (29) and substituting the expression of (28), we obtain:

$$\begin{aligned} \dot{s}_2 &= \dot{e}_2^\theta + c_7 \dot{e}_1^\theta + c_8 \alpha_\theta |\dot{e}_1^\theta|^{\alpha_\theta - 1} + c_9 \beta_\theta |\dot{e}_1^\theta|^{\beta_\theta - 1} \\ &= g(\theta)u_2 + d_\theta(t) - \ddot{\theta}_d + c_7 \dot{e}_1^\theta + c_8 \alpha_\theta |\dot{e}_1^\theta|^{\alpha_\theta - 1} + c_9 \beta_\theta |\dot{e}_1^\theta|^{\beta_\theta - 1} \end{aligned} \tag{30}$$

to ensure fast reach of the sliding manifold, we use the exponential approach law, defined as:

$$\dot{s}_2 = -k_1^{s_2} s_2 - k_\theta \mathrm{sign}(s_2) \tag{31}$$

here $k_1^{s_2}$ and k_θ are two positive-definite parameters, with k_θ being adjusted using a neural network in the following section.

Therefore, combining expressions (30) and (31), we design the orientation control law of the mobile robot as:

$$u_2 = \frac{1}{g(\theta)}\left[\ddot{\theta}_d - \widehat{d_\theta} - c_7 \dot{e}_1^\theta - c_8 \alpha_\theta |\dot{e}_1^\theta|^{\alpha_\theta - 1} - c_9 \beta_\theta |\dot{e}_1^\theta|^{\beta_\theta - 1} - k_1^{s_2} s_2 - k_\theta \mathrm{sign}(s_2) \right] \tag{32}$$

2.2.4. Design of adaptive laws

In this section, a neural network is employed to dynamically adjust the sliding surface coefficients in real-time. Specifically, the coefficients $\hat{c}_i > 0$ for $i = \overline{1,9}$ and $\hat{k}_l > 0$ for $l = \overline{x, y, \theta}$ are adjusted, where $\hat{c}_i$ and $\hat{k}_l$ represent the estimates of c_i and k_l respectively. This approach aims to minimize tracking errors and mitigate the chattering phenomenon. The neural network is trained using an online specialized learning architecture [29], [30], which uses the backpropagation algorithm to dynamically adapt the coefficients of the sliding surfaces. To this end, we initially design the adaptive laws for the coefficients $\hat{c}_i > 0, \; i = \overline{1,3}$ and $\hat{k}_x$ through the following steps:

- First, we establish the performance error $E_x = \frac{1}{2}\big[x - x_d\big]^2$, which is formulated as a function of the difference between the desired state and the current state of the mobile robot.

- Using the steepest descent approach [29], we derive the following adaptive equations:

$$\hat{k}_x = k_{x,0} - \omega \int_0^t \frac{\partial E_x}{\partial \hat{k}_x}, \hat{c}_1 = c_{1,0} - \omega \int_0^t \frac{\partial E_x}{\partial \hat{c}_1}, \hat{c}_2 = c_{2,0} - \omega \int_0^t \frac{\partial E_x}{\partial \hat{c}_2}, \hat{c}_3 = c_{3,0} - \omega \int_0^t \frac{\partial E_x}{\partial \hat{c}_3}, \quad (33)$$

where ω is the learning rate, $k_{x,0}, c_{1,0}, c_{2,0}$ and $c_{3,0}$ are initial values of $\hat{k}_x, \hat{c}_1, \hat{c}_2$ and $\hat{c}_3$ respectively.
- By applying the chain rule for partial derivatives, the following expressions can be derived:

$$
\begin{aligned}
\frac{\partial E_x}{\partial \hat{k}_x} &= \frac{\partial E_x}{\partial x} \frac{\partial x}{\partial u_{eq}^x} \frac{\partial u_{eq}^x}{\partial \hat{k}_x} = -(e_1^x)\text{sign}\left(\frac{\Delta x}{\Delta u_{eq}^x}\right) \frac{1}{g_1(X)}\text{sign}(\sigma_x), \\
\frac{\partial E_x}{\partial \hat{c}_1} &= \frac{\partial E_x}{\partial x} \frac{\partial x}{\partial u_{eq}^x} \frac{\partial u_{eq}^x}{\partial \sigma_x} \frac{\partial \sigma_x}{\partial \hat{c}_1} = -\text{sign}\left(\frac{\Delta x}{\Delta \partial u_{eq}^x}\right) \frac{1}{g_1(X)}\left(\frac{4e^{-2\sigma_x}k_x}{(1+e^{-2\sigma_x})^2}\right)(e_1^x)^2, \\
\frac{\partial E_x}{\partial \hat{c}_2} &= \frac{\partial E_x}{\partial x} \frac{\partial x}{\partial u_{eq}^x} \frac{\partial u_{eq}^x}{\partial \sigma_x} \frac{\partial \sigma_x}{\partial \hat{c}_2} = -\text{sign}\left(\frac{\Delta x}{\Delta u_{eq}^x}\right) \frac{1}{g_1(X)}\left(\frac{4e^{-2\sigma_x}k_x}{(1+e^{-2\sigma_x})^2}\right)|e_1^x|^{\alpha_x+1}\text{sign}(e_1^x), \\
\frac{\partial E_x}{\partial \hat{c}_3} &= \frac{\partial E_x}{\partial x} \frac{\partial x}{\partial u_{eq}^x} \frac{\partial u_{eq}^x}{\partial \sigma_x} \frac{\partial \sigma_x}{\partial \hat{c}_3} = -\text{sign}\left(\frac{\Delta x}{\Delta u_{eq}^x}\right) \frac{1}{g_1(X)}\left(\frac{4e^{-2\sigma_x}k_x}{(1+e^{-2\sigma_x})^2}\right)|e_1^x|^{\beta_x+1}\text{sign}(e_1^x).
\end{aligned}
\quad (34)
$$

- Substituting (34) into (33), the adaptive coefficients of the sliding surface σ_x are designed as follows:

$$
\begin{aligned}
\hat{k}_x &= k_{x,0} + \omega \int_0^t (e_1^x)\text{sign}\left(\frac{\Delta x}{\Delta u_{eq}^x}\right) \frac{1}{g_1(X)}\text{sign}(\sigma_x), \\
\hat{c}_1 &= c_{1,0} + \omega \int_0^t \text{sign}\left(\frac{\Delta x}{\Delta \partial u_{eq}^x}\right) \frac{1}{g_1(X)}\left(\frac{4e^{-2\sigma_x}\hat{k}_x}{(1+e^{-2\sigma_x})^2}\right)(e_1^x)^2, \\
\hat{c}_2 &= c_{2,0} + \omega \int_0^t \text{sign}\left(\frac{\Delta x}{\Delta u_{eq}^x}\right) \frac{1}{g_1(X)}\left(\frac{4e^{-2\sigma_x}\hat{k}_x}{(1+e^{-2\sigma_x})^2}\right)|e_1^x|^{\alpha_x+1}\text{sign}(e_1^x), \\
\hat{c}_3 &= c_{3,0} + \omega \int_0^t \text{sign}\left(\frac{\Delta x}{\Delta u_{eq}^x}\right) \frac{1}{g_1(X)}\left(\frac{4e^{-2\sigma_x}\hat{k}_x}{(1+e^{-2\sigma_x})^2}\right)|e_1^x|^{\beta_x+1}\text{sign}(e_1^x).
\end{aligned}
\quad (35)
$$

where Δ refers to the upward difference operator, defined as $\nabla\zeta_k = \zeta_k - \zeta_{k-1}$ [29].

By applying the same method as in the earlier steps, the coefficients for the sliding surfaces σ_y and s_θ are determined as follows:

$$
\begin{cases}
\hat{k}_y = k_{y,0} + \omega \int_0^t \frac{\Xi_y(e_1^y)}{g_2(X)}\text{sign}(\sigma_y), \\
\hat{c}_4 = c_{4,0} + \omega \int_0^t \frac{\Xi_y(e_1^y)^2}{g_2(X)}\left(\frac{4e^{-2\sigma_y}\hat{k}_y}{(1+e^{-2\sigma_y})^2}\right), \\
\hat{c}_5 = c_{5,0} + \omega \int_0^t \frac{\Xi_y\text{sign}^{\alpha_y+1}(e_1^y)}{g_2(X)}\left(\frac{4e^{-2\sigma_y}\hat{k}_y}{(1+e^{-2\sigma_y})^2}\right), \\
\hat{c}_6 = c_{6,0} + \omega \int_0^t \frac{\Xi_y\text{sign}^{\beta_y+1}(e_1^y)}{g_2(X)}\left(\frac{4e^{-2\sigma_y}\hat{k}_y}{(1+e^{-2\sigma_y})^2}\right).
\end{cases}
\begin{cases}
\hat{k}_\theta = k_{\theta,0} + \omega \int_0^t \frac{\Xi_\theta(e_1^\theta)}{g_2(\theta)}\text{sign}(s_\theta), \\
\hat{c}_7 = c_{7,0} + \omega \int_0^t \frac{\Xi_\theta(e_1^\theta)^2}{g_2(\theta)}\left(\frac{4e^{-2s_\theta}\hat{k}_\theta}{(1+e^{-2s_\theta})^2}\right), \\
\hat{c}_8 = c_{8,0} + \omega \int_0^t \frac{\Xi_\theta\text{sign}^{\alpha_\theta+1}(e_1^\theta)}{g_2(\theta)}\left(\frac{4e^{-2s_\theta}\hat{k}_\theta}{(1+e^{-2s_\theta})^2}\right), \\
\hat{c}_9 = c_{9,0} + \omega \int_0^t \frac{\Xi\text{sign}^{\beta_\theta+1}(e_1^\theta)}{g_2(\theta)}\left(\frac{4e^{-2s_\theta}\hat{k}_\theta}{(1+e^{-2s_\theta})^2}\right).
\end{cases}
\quad (36)
$$

where $\Xi_y = \text{sign}\left(\frac{\Delta y}{\Delta u_{eq}^y}\right), \Xi_\theta = \text{sign}\left(\frac{\Delta \theta}{\Delta u_2}\right)$.

The adaptive laws developed in (35) and (36), together with the estimation of the external disturbances in (7) and the control laws defined in (24) and (32), form a robust and efficient control system for trajectory tracking in a 3WMR. Algorithm 1, which details the necessary steps to implement the control system proposed.

Algorithm 1. Algorithm of the proposed control system

1: **Input:**
2: Define the physical characteristics of the mobile robot: m, J, r, L
3: Define the parameters of the FTDO observer: ξ_1, ξ_2, ξ_3, L_q
4: Define the parameters of the control strategy: $\alpha_x, \alpha_y, \alpha_\theta, \beta_x, \beta_y, \beta_\theta, \eta_1, \eta_2, k_1^{s1}, k_1^{s2}$
5: Define the adaptive parameters for the neural network: $k_{x,0}, k_{y,0}, k_{\theta,0}, c_{1,0}, c_{2,0}, c_{3,0}, c_{4,0}, c_{5,0}, c_{6,0}, c_{7,0}, c_{8,0}, c_{9,0}$
6: **while** Repeat **do**
7:     **Underactuated Control System**
8:     Acquire the current states: $x, \dot{x}, y, \dot{y}$
9:     Compute the tracking errors: $e_1^x, e_2^x, e_1^y, e_2^y$
10:    Define the neural network performance error: E_x, E_y
11:    Calculate the adaptive parameters for the sliding surface: $\hat{k}_x, \hat{k}_y, \hat{c}_1, \hat{c}_2, \hat{c}_3, \hat{c}_4, \hat{c}_5, \hat{c}_6$
12:    Define the sliding surfaces of the first layer in the hierarchical structure: σ_x, σ_y
13:    Time derivative of the sliding surfaces of the first layer: $\dot{\sigma}_x, \dot{\sigma}_y$
14:    Calculate the equivalent control laws: u_{eq}^x, u_{eq}^y
15:    Define the sliding surface of the second layer in the hierarchical structure: s_1
16:    Time derivative of the sliding surface of the second layer: $\dot{s}_1$
17:    Calculate the switching control law: $u_{sw}^{x,y}$
18:    Calculate the position control law: u_1
19:    **Fully Actuated Control System**
20:    Acquire the current states: $\theta, \dot{\theta}$
21:    Calculate the tracking errors: e_1^θ, e_2^θ
22:    Define the neural network performance error: E_θ
23:    Calculate the adaptive parameters for the sliding surface: $\hat{k}_\theta, \hat{c}_7, \hat{c}_8, \hat{c}_9$
24:    Define the sliding surface: s_2
25:    Time derivative of the sliding surfaces: $\dot{s}_2$
26:    Calculate the orientation control law: u_2
27:    **FTDO Observer**
28:    Acquire the control inputs: u_1, u_2
29:    Acquire the current states: $x, \dot{x}, y, \dot{y}, \theta, \dot{\theta}$
30:    Calculate the disturbance estimations: $\hat{d}_x(t), \hat{d}_y(t), \hat{d}_\theta(t)$
31: **end while**

2.3. Stability analysis

- Theorem 2 considering the dynamical system in (25), together with the control law designed in (32) and the design of the adaptive laws defined in (36), then the system states will reach the sliding surface in a finite time. As a result, the tracking errors in (27) will approach zero in a finite time.

- Proof 2 considering the following Lyapunov candidate function as:

$$V = \frac{1}{2}(e_1^\theta)^2 + \frac{1}{2}(s_2)^2 + \frac{1}{2}(\widetilde{k}_\theta)^2 + \frac{1}{2}(\widetilde{c}_7)^2 + \frac{1}{2}(\widetilde{c}_8)^2 + \frac{1}{2}(\widetilde{c}_9)^2 \tag{37}$$

where $\widetilde{c}_i, (i = 7, 8, 9)$ is the adaptive estimation error, then $\widetilde{c}_i = \hat{c}_i - c_i$. Deriving in time (37), we obtain:

$$\dot{V} = e_1^\theta(e_2^\theta) + s_2(\dot{s}_2) + \widetilde{k}_\theta(\dot{\hat{k}}_\theta) + \widetilde{c}_7(\dot{\hat{c}}_7) + \widetilde{c}_8(\dot{\hat{c}}_8) + \widetilde{c}_9(\dot{\hat{c}}_9) \tag{38}$$

Substituting the expressions of (28) and (30) into (38), we obtain the following:

$$\dot{V} = e_1^\theta(-\hat{c}_7 e_1^\theta - \hat{c}_8|e_1^\theta|^{\alpha_\theta}\operatorname{sgn}(e_1^\theta) - \hat{c}_9|e_1^\theta|^{\beta_\theta}\operatorname{sgn}(e_1^\theta)) + \\ s_2(-k_1^{s2}s_2 - \hat{k}_\theta\operatorname{sign}(s_2)) + \widetilde{k}_\theta(\dot{\hat{k}}_\theta) + \widetilde{c}_7(\dot{\hat{c}}_7) + \widetilde{c}_8(\dot{\hat{c}}_8) + \widetilde{c}_9(\dot{\hat{c}}_9) \tag{39}$$

By performing some mathematical operations and adding and subtracting some terms, the following expression is obtained:

$$\dot{V} = -\hat{c}_7|e_1^\theta|^2 - \hat{c}_8|e_1^\theta|^{\alpha_\theta+1} - \hat{c}_9|e_1^\theta|^{\beta_\theta+1} - k_1^{s2}|s_2|^2 - \hat{k}_\theta|s_2| + \widetilde{k}_\theta(\dot{\hat{k}}_\theta) + \widetilde{c}_7(\dot{\hat{c}}_7) + \widetilde{c}_8(\dot{\hat{c}}_8) + \\ \widetilde{c}_9(\dot{\hat{c}}_9) + c_7|e_1^\theta|^2 - c_7|e_1^\theta|^2 + c_8|e_1^\theta|^{\alpha_\theta+1} - c_8|e_1^\theta|^{\alpha_\theta+1} + c_9|e_1^\theta|^{\beta_\theta+1} - c_9|e_1^\theta|^{\beta_\theta+1} + k_\theta|s_2| - k_\theta|s_2| \\ = -\widetilde{c}_7|e_1^\theta|^2 - \widetilde{c}_8|e_1^\theta|^{\alpha_\theta+1} - \widetilde{c}_9|e_1^\theta|^{\beta_\theta+1} - \widetilde{k}_\theta|s_2| - k_1^{s2}|s_2|^2 + \widetilde{k}_\theta(\dot{\hat{k}}_\theta) + \widetilde{c}_7(\dot{\hat{c}}_7) + \widetilde{c}_8(\dot{\hat{c}}_8) + \widetilde{c}_9(\dot{\hat{c}}_9) - \\ k_\theta|s_2| - c_7|e_1^\theta|^2 - c_8|e_1^\theta|^{\alpha_\theta+1} - c_9|e_1^\theta|^{\beta_\theta+1} \tag{40}$$

Putting together some common terms, we obtain:

$$\dot{V} = -(c_7 + c_8|e_1^\theta|^{\alpha_\theta-1} + c_9|e_1^\theta|^{\beta_\theta-1})|e_1^\theta|^2 - (k_1^{s2} + k_\theta/s_2)|s_2|^2 - (|s_2| - \dot{\hat{k}}_\theta)|\widetilde{k}_\theta| - \\ (|e_1^\theta|^2 - \dot{\hat{c}}_7)|\widetilde{c}_7| - (|e_1^\theta|^{\alpha_\theta+1} - \dot{\hat{c}}_8)|\widetilde{c}_8| - (|e_1^\theta|^{\beta_\theta+1} - \dot{\hat{c}}_9)|\widetilde{c}_9| \tag{41}$$

To simplify the expression, we define the following variables:

$$\begin{aligned}
\Phi_1 &= (c_7 + c_8|e_1^\theta|^{\alpha_\theta-1} + c_9|e_1^\theta|^{\beta_\theta-1}), \Phi_2 = (k_1^{s_2} + k_\theta/s_2), \Phi_3 = (|s_2| - \dot{\tilde{k}}_\theta), \\
\Phi_4 &= (|e_1^\theta|^2 - \dot{\tilde{c}}_7), \Phi_5 = (|e_1^\theta|^{\alpha_\theta+1} - \dot{\tilde{c}}_8), \Phi_6 = (|e_1^\theta|^{\beta_\theta+1} - \dot{\tilde{c}}_9)
\end{aligned} \tag{42}$$

According to (42), the (41) is obtained:

$$\dot{V} = -\Phi_1|e_1^\theta|^2 - \Phi_2|s_2|^2 - \Phi_3|\tilde{k}_\theta| - \Phi_4|\tilde{c}_7| - \Phi_5|\tilde{c}_8| - \Phi_6|\tilde{c}_9| \tag{43}$$

Performing some mathematical adjustments, we obtain the following:

$$\dot{V} = -\Phi_1|e_1^\theta|^2 - \Phi_2|s_2|^2 - \sqrt{2}\Phi_3\left(\frac{|\tilde{k}_\theta|^2}{2}\right)^\varepsilon - \sqrt{2}\Phi_4\left(\frac{|\tilde{c}_7|^2}{2}\right)^\varepsilon - \sqrt{2}\Phi_5\left(\frac{|\tilde{c}_8|^2}{2}\right)^\varepsilon - \sqrt{2}\Phi_6\left(\frac{|\tilde{c}_9|^2}{2}\right)^\varepsilon \tag{44}$$

where $\varepsilon = 1/2$. Now, according to Lemma 3 of [31] and grouping common terms, we obtain:

$$\begin{aligned}
\dot{V} =& -\Phi_1\left[\left(\frac{|e_1^\theta|^2}{2}\right)^\varepsilon - (1-\varepsilon)\varepsilon^{\frac{\varepsilon}{1-\varepsilon}}\right] - \Phi_2\left[\left(\frac{|s_2|^2}{2}\right)^\varepsilon - (1-\varepsilon)\varepsilon^{\frac{\varepsilon}{1-\varepsilon}}\right] - \\
& - \sqrt{2}\Phi_3\left(\frac{|\tilde{k}_\theta|^2}{2}\right)^\varepsilon - \sqrt{2}\Phi_4\left(\frac{|\tilde{c}_7|^2}{2}\right)^\varepsilon - \sqrt{2}\Phi_5\left(\frac{|\tilde{c}_8|^2}{2}\right)^\varepsilon - \sqrt{2}\Phi_6\left(\frac{|\tilde{c}_9|^2}{2}\right)^\varepsilon \\
=& -\Phi_1\left(\frac{|e_1^\theta|^2}{2}\right)^\varepsilon - \Phi_2\left(\frac{|s_2|^2}{2}\right)^\varepsilon - \sqrt{2}\Phi_3\left(\frac{|\tilde{k}_\theta|^2}{2}\right)^\varepsilon - \sqrt{2}\Phi_4\left(\frac{|\tilde{c}_7|^2}{2}\right)^\varepsilon - \\
& \sqrt{2}\Phi_5\left(\frac{|\tilde{c}_8|^2}{2}\right)^\varepsilon - \sqrt{2}\Phi_6\left(\frac{|\tilde{c}_9|^2}{2}\right)^\varepsilon + (\Phi_1 + \Phi_2)(1-\varepsilon)\varepsilon^{\frac{\varepsilon}{1-\varepsilon}} = -K_V V^\varepsilon + P_V
\end{aligned} \tag{45}$$

where $K_V = \left\{\Phi_1, \Phi_2, \sqrt{2}\Phi_3, \sqrt{2}\Phi_4, \sqrt{2}\Phi_5, \sqrt{2}\Phi_6\right\}$ and $P_V = \left\{(\Phi_1 + \Phi_2)(1-\varepsilon)\varepsilon^{\frac{\varepsilon}{1-\varepsilon}}\right\}$.

Therefore, according to Lemma 4 of [32] and for any $0 < \varrho < 1$, it can be inferred that the errors in (34) can be stabilized to zero during the sliding motion $s_2 = 0$ in a finite time T_f defined by:

$$T_f = \frac{1}{(1-\varepsilon)\varrho K_V}\left(V^{1-\varepsilon}(0) - \left(\frac{P_V}{(1-\varrho)K_V}\right)^{\frac{1-\varepsilon}{\varepsilon}}\right). \tag{46}$$

Thus, completing the proof.

- Remark 1 following the same procedure as in the proof of Theorem 2, it can be demonstrated that the tracking errors in (13) stabilize to zero during the motion of the sliding surface $s_1 = 0$ in finite time.

Figure 3 shows the simulation setup of the control system proposed in this paper, implemented in MATLAB/Simulink software (version 2021a). The setup includes several blocks developed in this section, such as the dynamic modeling of the 3WMR, the FTDO observer, the control strategy and the adaptive neural network scheme.
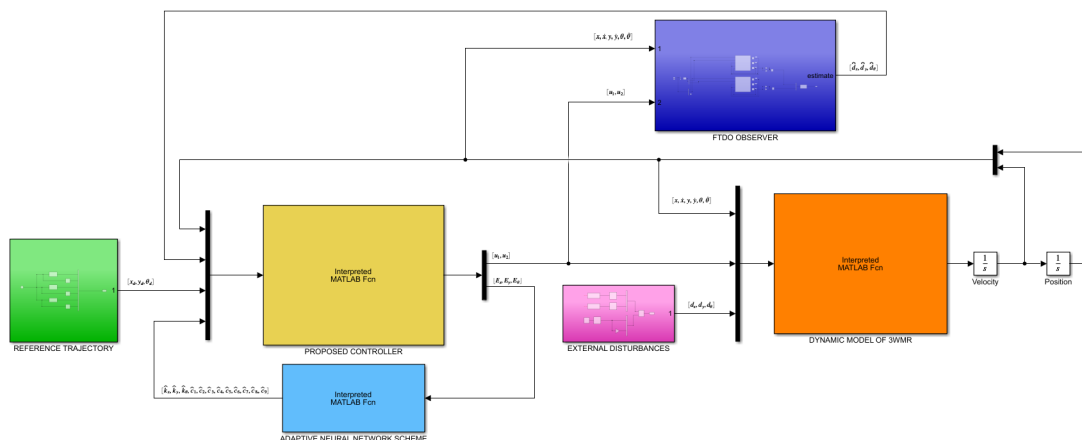

Figure 3. Simulation setup of the proposed control system in MATLAB/Simulink

3.   RESULTS AND DISCUSSION

In this section, the proposed control system, designed in the previous section, is validated through numerical simulations performed using MATLAB/Simulink software (version 2021a). The simulations were executed on a Lenovo laptop with 8 GB of RAM, a 9th generation Intel Core i5 processor, and 466 GB of SSD storage. To evaluate convergence time, tracking accuracy, and disturbance rejection capabilities, a comparative study is conducted between our proposed control system, AHFTSMC, and two hierarchical control schemes: HFSMAC [25] and adaptive backstepping hierarchical sliding mode control (ABHSMC) [27]. The parameters of the mobile robot and the control system are detailed in Tables 1 and 2, respectively.

Table 1. 3WMR parameters

Parameters	m	J	r	L
Value	4 Kg	2.5 Kg/m^2	0.04 m	0.2 m

Table 2. Control system parameters

Parameter	Value	Parameter	Value	Parameter	Value	Parameter	Value	Parameter	Value
ξ_1	5	$c_{1,0}$	12	$c_{5,0}$	2.5	$c_{9,0}$	1.2	β_x	2.5
ξ_2	8	$c_{2,0}$	2.5	$c_{6,0}$	2.5	α_x	2.1	β_y	1.5
ξ_3	6	$c_{3,0}$	2.5	$c_{7,0}$	8	α_y	1.2	β_θ	1.5
L_q	3	$c_{4,0}$	12	$c_{8,0}$	1.2	α_θ	0.8	$k_1^{s_1}, k_1^{s_2}$	5

3.1.   Trajectory tracking of a straight line

The reference trajectory for this scenario is set as follows:

$$q_d = [x_d, y_d, \theta_d]^T = [0.25t, 0.25t, \pi/4]^T$$

In this case, only external disturbances are considered, given by $d(t) = [d_x, d_y] = [1.2, -1.2]^T$. These disturbances are introduced to the dynamic system at specific time instants. Since the 3WMR is an underactuated system with coupled dynamics, external position disturbances inevitably affect the orientation of the mobile robot.

The results are presented in Figures 4-6. Figure 4(a) shows the 3D simulation of the mobile robot trajectory tracking with the different controllers, while Figure 4(b) shows a 2D view of the trajectory tracking of the 3WMR. An initial analysis of these figures clearly demonstrates that our proposed control system exhibits superior trajectory tracking performance compared to the HFSMAC and ABHSMC approaches.

(a)   (b)
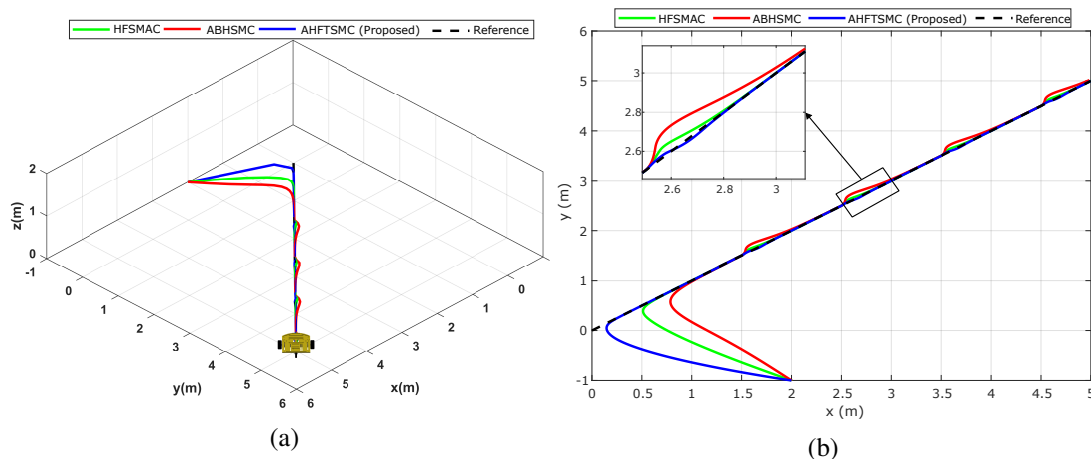
Figure 4. Trajectory tracking response under different controllers, (a) viewed in 3D and (b) viewed in 2D

Figure 5(a) presents the temporal response of the Cartesian position and orientation, demonstrating faster convergence of our proposed control system across all three states of the mobile robot compared to the HFSMAC and ABHSMC controllers. It also highlights the improved tracking accuracy of our approach,

which is particularly evident in the zoomed-in regions, even in the presence of external disturbances. In Figure 5(b), the tracking errors are displayed, highlighting the outstanding ability of our system to reject external disturbances. This results in greater robustness, as the errors converge to zero and remain consistently near the origin, unlike the HFSMAC and ABHSMC controllers, which are clearly affected by these disturbances. The control inputs are shown in Figure 6(a). Finally, Figure 6(b) illustrates the response of the FTDO, where the designed observer accurately identifies the external disturbances acting on the mobile robot. These disturbances are effectively compensated by the control system, further improving disturbance rejection.
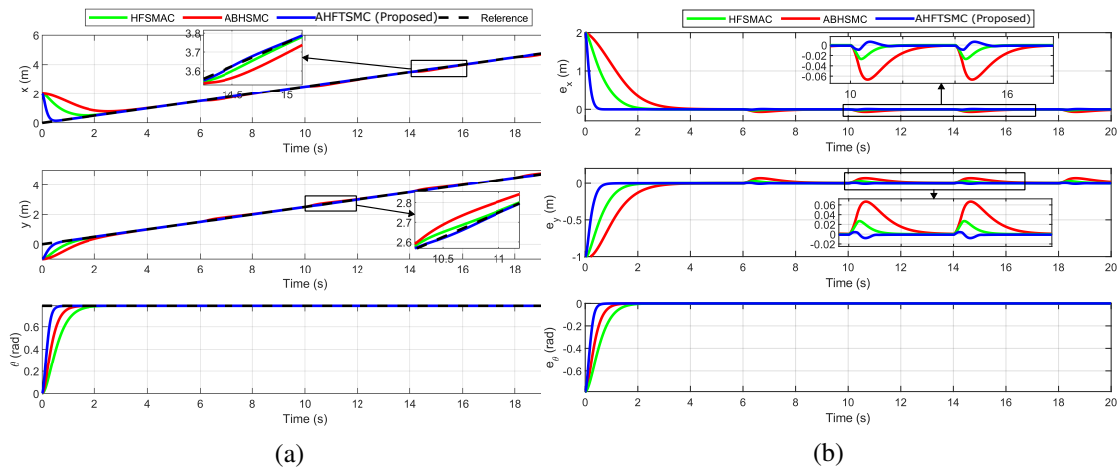
Figure 5. Temporal response of (a) position and (b) tracking errors
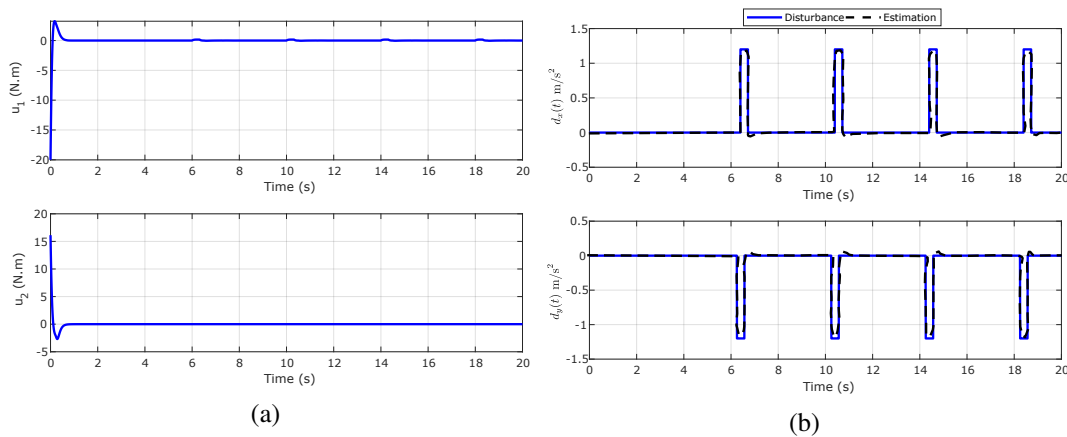
Figure 6. Temporal response of (a) control inputs and (b) FTDO estimation

In this study, we use the performance indices of settling time, root mean squared error (RMSE), and integral squared error (ISE) to provide a more accurate quantitative comparison between the results of our proposed control system and those of the HFSMAC and ABHSMC controllers. These indices are calculated and compiled in Table 3, with the top results emphasized in bold. Table 3 compares the settling times of our proposed control system with those of the HFSMAC and ABHSMC controllers. The results show that our approach achieves shorter settling times, confirming its exceptional ability to ensure fast convergence in finite time. Additionally, Table 3 presents a comparison of the RMSE and ISE indices, where our control system consistently achieves lower values than the HFSMAC and ABHSMC controllers, reaffirming the superiority of our approach in terms of tracking accuracy. To further aid in interpreting these results, the RMSE and ISE values are visualized in a bar chart, as shown in Figure 7.

Table 3. Analysis of performance indices for scenario 1

Control strategy	Settling time			RMSE			ISE		
	x	y	θ	x	y	θ	x	y	θ
HFSMAC	1.984	1.857	1.635	0.296	0.154	0.139	1.752	0.474	0.386
ABHSMC	3.435	3.586	0.912	0.419	0.219	0.114	3.511	0.959	0.259
AHFTSMC (proposed)	0.692	0.645	0.548	0.151	0.095	0.059	0.456	0.180	0.109

Figure 7(a) presents the RMSE values for the three control approaches: HFSMAC, ABHSMC and the proposed control. It can be seen that the RMSE values of the proposed approach are lower compared to the other control approaches. In particular, the RMSE values of the proposed controller are 0.151 in x, 0.095 in y, and 0.059 in θ. Figure 7(b) shows the ISE values for the same controllers and state variables. As in Figure 7(a), the proposed control approach exhibits the lowest ISE values, with 0.456 in x, 0.180 in y and 0.109 in θ.

(a)   (b)
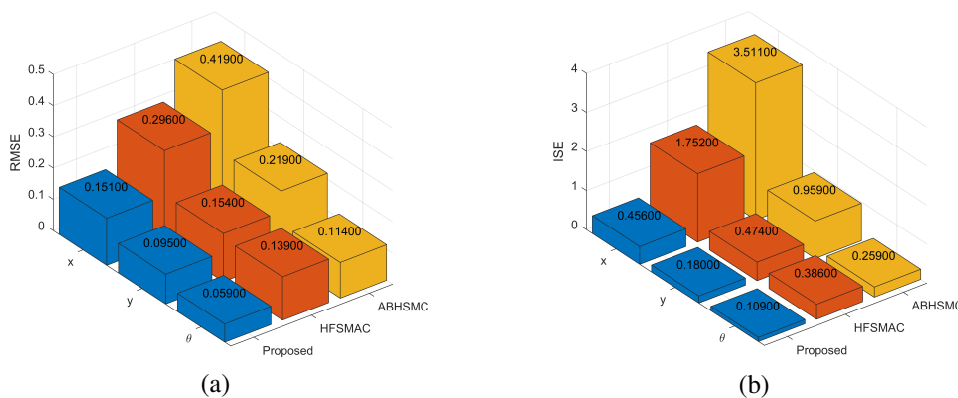
Figure 7. Performance indices (a) RMSE and (b) ISE

3.2. Trajectory tracking of a sine curve

The reference trajectory is set as follows:

$$q_d = [1 + 0.2t, 1 + 0.25\sin(0.2\pi t), \text{atan}(0.25\pi\cos(0.2\pi t))]^T \tag{47}$$

In this case, we consider both external and internal disturbances during the motion of the mobile robot. These lumped disturbances are defined as:

a) External disturbances: assume the mobile robot arrives a challenging environment at time $t = 8$ seconds with the presence of the following external disturbances:

$$d(t) = [d_x, d_y] = [0.5\sin(3t) + 0.8\cos(2t), -1.2\cos(3t) + 0.2\sin(5t) - 0.5\cos(2t)]^T \tag{48}$$

b) Internal disturbances: represents the variation of the physical characteristics of the mobile robot; for this, we consider parametric uncertainties of 30% in the mass and moment of inertia of the mobile robot.

The findings are displayed in Figures 8-10. Figure 8(a) illustrates the 3D simulation of the 3WMR following the reference trajectory with the different controllers, while Figure 8(b) provides a 2D view of the trajectory tracking of the 3WMR under the presence of both external and internal disturbances. From these figures, it is evident that, similar to the previous scenario, our suggested control approach achieves superior performance compared to HFSMAC and ABHSMC controllers in trajectory tracking even in the presence of large lumped disturbances.

The temporal response of the Cartesian position and orientation are plotted in Figure 9(a). As in the previous case, our proposed control system demonstrates fast convergence in all three states of the mobile robot to the reference signal, while also exhibiting accurate tracking and remarkable disturbance rejection compared to the HFSMAC and ABHSMC controllers. This superiority is clearly evident in Figure 9(b), where the tracking errors converge to zero and remain consistently near the origin despite large external and internal

disturbances. In contrast, the HFSMAC and ABHSMC controllers are significantly affected by lumped disturbances, as shown in the zoomed-in regions of tracking errors in Figure 9(b). The control inputs are presented in Figure 10(a). Finally, Figure 10(b) displays the response of the FTDO, where it is observed that the designed observer accurately identifies the lumped disturbances affecting the mobile robot at $t = 8$ seconds. These disturbances are effectively compensated by the control system, significantly enhancing the system's disturbance rejection capability. As a result, the mobile robot follows the reference trajectory smoothly despite the lumped disturbances, as illustrated in Figure 8.
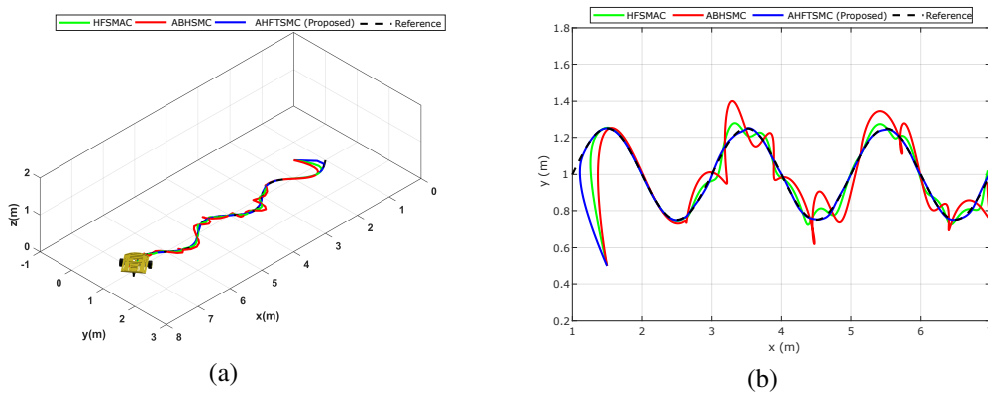
Figure 8. Trajectory tracking response under different controllers, (a) viewed in 3D and (b) viewed in 2D
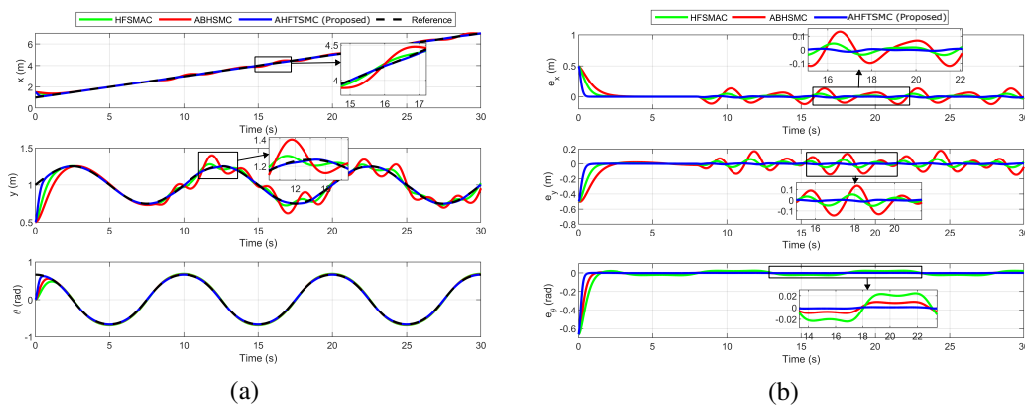
Figure 9. Temporal response of (a) position and (b) tracking errors of scenario 2
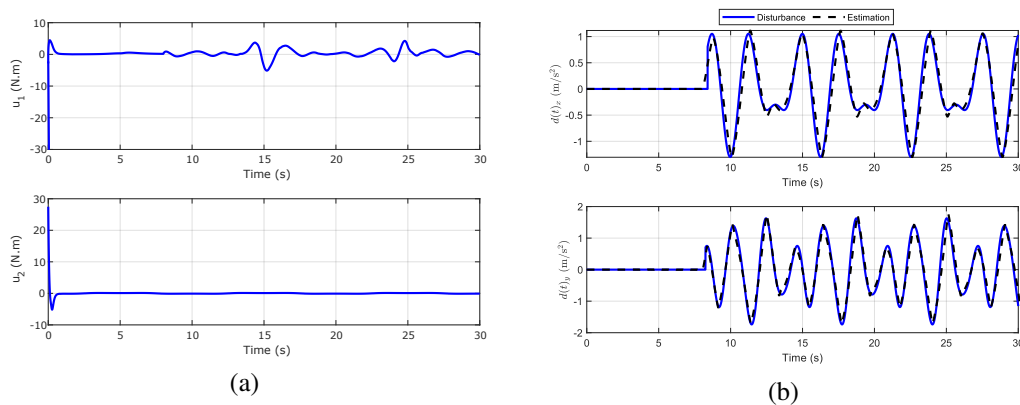
Figure 10. Temporal response of (a) control inputs and (b) FTDO estimation of scenario 2

For a more precise comparative analysis, the performance indices described above were calculated. The calculations are presented in Table 4. From this table, it is clear that our proposed control approach offers superior performance in tracking the trajectory of a 3WMR, even in the presence of large disturbances. The settling times, as well as the RMSE and ISE values, are lower compared to those of the HFSMAC and ABHSMC controllers. These results highlight the excellent characteristics of the proposed control system, which is noted for its rapid convergence, high tracking accuracy, and remarkable ability to reject disturbances. To facilitate the interpretation of these results, the RMSE and ISE values are presented in a bar chart, as illustrated in Figure 11.

Figure 11(a) presents the RMSE values for the three control approaches under the presence of both external and internal disturbances. It is evident that the RMSE values of the proposed approach are lower compared to the other control approaches. In particular, the RMSE values of the proposed controller are 0.266 in x, 0.189 in y, and 0.124 in θ. Figure 11(b) shows the ISE values for the same controllers and state variables. As in Figure 11(a), the proposed control approach exhibits the lowest ISE values, with 0.471 in x, 0.265 in y and 0.214 in θ.

Table 4. Analysis of performance indices for scenario 2

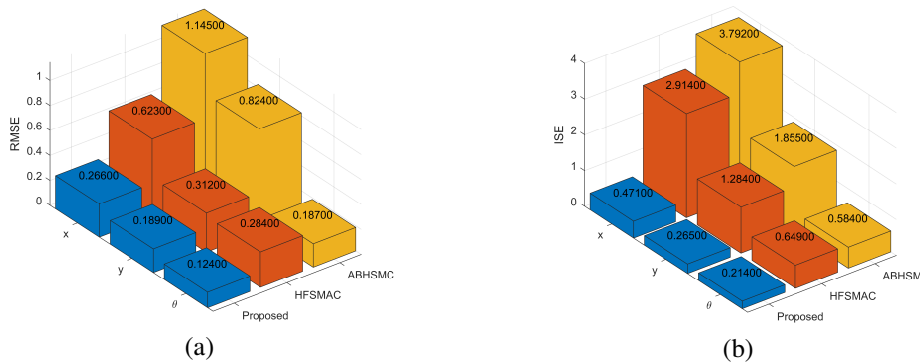| Control strategy	Settling time			RMSE			ISE		
	x	y	θ	x	y	θ	x	y	θ
HFSMAC	2.184	2.432	2.182	0.623	0.312	0.284	2.914	1.284	0.649
ABHSMC	3.692	3.927	1.712	1.145	0.824	0.187	3.792	1.855	0.584
AHFTSMC (proposed)	0.814	0.914	0.711	0.266	0.189	0.124	0.471	0.265	0.214

Figure 11. Performance indices (a) RMSE and (b) ISE

4. CONCLUSION

This research presented the design of a novel neuro-adaptive HSMC system for trajectory tracking of a 3WMR subjected to large lumped disturbances. The validation of the proposed system was carried out by numerical simulations in MATLAB/Simulink, comparing its performance with the HSMC, HFSMAC, and ABHSMC. The obtained results, supported by a quantitative comparative analysis, have confirmed the superiority of our proposed control approach in terms of fast convergence, higher tracking accuracy and better disturbance rejection capability compared to HFSMAC and ABHSMC controllers. Future work will focus on the experimental validation of the control system and the integration of potential field algorithms for obstacle avoidance.

REFERENCES

[1] F. Rubio, F. Valero, and C. Llopis-Albert, "A review of mobile robots: concepts, methods, theoretical framework, and applications," *International Journal of Advanced Robotic Systems*, vol. 16, no. 2, Mar. 2019, doi: 10.1177/1729881419839596.
[2] M. Z. K. Hawari and N. I. A. Apandi, "Industry 4.0 with intelligent manufacturing 5G mobile robot based on genetic algorithm," *Indonesian Journal of Electrical Engineering and Computer Science (IJEECS)*, vol. 23, no. 3, pp. 1376–1384, Sep. 2021, doi: 10.11591/ijeecs.v23.i3.pp1376-1384.
[3] N. A. Martins and D. W. Bertol, *Wheeled mobile robot control*, vol. 380. Cham: Springer International Publishing, 2022.

[4] A. Alouache and Q. Wu, "Genetic algorithms for trajectory tracking of mobile robot based on PID controller," in *Proceedings - 2018 IEEE 14th International Conference on Intelligent Computer Communication and Processing, ICCP 2018*, Sep. 2018, pp. 237–241, doi: 10.1109/ICCP.2018.8516587.

[5] H. H. Ammar and A. T. Azar, "Robust path tracking of mobile robot using fractional order PID controller," *Advances in Intelligent Systems and Computing*, vol. 921, pp. 370–381, 2020, doi: 10.1007/978-3-030-14118-9_37.

[6] S. Morales, J. Magallanes, C. Delgado, and R. Canahuire, "LQR trajectory tracking control of an omnidirectional wheeled mobile robot," in *2018 IEEE 2nd Colombian Conference on Robotics and Automation, CCRA 2018*, Nov. 2018, pp. 1–5, doi: 10.1109/CCRA.2018.8588146.

[7] M. D. N. Forte, W. B. Correia, F. G. Nogueira, and B. C. Torrico, "Reference tracking of a nonholonomic mobile robot using sensor fusion techniques and linear control," *IFAC-PapersOnLine*, vol. 51, no. 4, pp. 364–369, 2018, doi: 10.1016/j.ifacol.2018.06.092.

[8] O. Mechali, L. Xu, Y. Huang, M. Shi, and X. Xie, "Observer-based fixed-time continuous nonsingular terminal sliding mode control of quadrotor aircraft under uncertainties and disturbances for robust trajectory tracking: theory and experiment," *Control Engineering Practice*, vol. 111, p. 104806, Jun. 2021, doi: 10.1016/j.conengprac.2021.104806.

[9] L. F. C. Ccari, P. R. Yanyachi, J. C. C. Luque, and D. Yanyachi, "Distributed robust adaptive control for finite-time flight formation of multi-quadcopter systems with large lumped uncertainties," *IEEE Access*, vol. 12, pp. 113384–113405, 2024, doi: 10.1109/ACCESS.2024.3439414.

[10] T. Elmokadem, M. Zribi, and K. Youcef-Toumi, "Trajectory tracking sliding mode control of underactuated AUVs," *Nonlinear Dynamics*, vol. 84, no. 2, pp. 1079–1091, Apr. 2016, doi: 10.1007/s11071-015-2551-x.

[11] I. Matraji, A. Al-Durra, A. Haryono, K. Al-Wahedi, and M. Abou-Khousa, "Trajectory tracking control of skid-steered mobile robot based on adaptive second order sliding mode control," *Control Engineering Practice*, vol. 72, pp. 167–176, Mar. 2018, doi: 10.1016/j.conengprac.2017.11.009.

[12] Z. Yuan, Y. Tian, Y. Yin, S. Wang, J. Liu, and L. Wu, "Trajectory tracking control of a four mecanum wheeled mobile platform: An extended state observer-based sliding mode approach," *IET Control Theory and Applications*, vol. 14, no. 3, pp. 415–426, Feb. 2020, doi: 10.1049/iet-cta.2018.6127.

[13] L. F. C. Ccari *et al.*, "Robust finite-time adaptive nonlinear control system for an EOD robotic manipulator: design, implementation, and experimental validation," *IEEE Access*, vol. 12, pp. 93859–93875, 2024, doi: 10.1109/ACCESS.2024.3424463.

[14] M. Labbadi, S. Boubaker, M. Djemai, S. K. Mekni, and A. Bekrar, "Fixed-time fractional-order global sliding mode control for nonholonomic mobile robot systems under external disturbances," *Fractal and Fractional*, vol. 6, no. 4, p. 177, Mar. 2022, doi: 10.3390/FRACTALFRACT6040177.

[15] M. Labbadi, S. Boubaker, S. Kamel, and F. S. Alsubaei, "Adaptive finite/fixed time control design for a class of nonholonomic systems with disturbances," *Mathematics*, vol. 11, no. 10, p. 2287, May 2023, doi: 10.3390/math11102287.

[16] N. K. Goswami and P. K. Padhy, "Sliding mode controller design for trajectory tracking of a non-holonomic mobile robot with disturbance," *Computers and Electrical Engineering*, vol. 72, pp. 307–323, Nov. 2018, doi: 10.1016/j.compeleceng.2018.09.021.

[17] H. Xie, J. Zheng, Z. Sun, H. Wang, and R. Chai, "Finite-time tracking control for nonholonomic wheeled mobile robot using adaptive fast nonsingular terminal sliding mode," *Nonlinear Dynamics*, vol. 110, no. 2, pp. 1437–1453, Oct. 2022, doi: 10.1007/s11071-022-07682-2.

[18] H. T. Sekban and A. Basci, "Designing new model-based adaptive sliding mode controllers for trajectory tracking control of an unmanned ground vehicle," *IEEE Access*, vol. 11, pp. 101387–101397, 2023, doi: 10.1109/ACCESS.2023.3313942.

[19] S. Liu, L. Zhang, B. Niu, X. Zhao, and A. M. Ahmad, "Adaptive neural finite-time hierarchical sliding mode control of uncertain under-actuated switched nonlinear systems with backlash-like hysteresis," *Information Sciences*, vol. 599, pp. 147–169, Jun. 2022, doi: 10.1016/j.ins.2022.03.077.

[20] D. Qian and J. Yi, "Hierarchical sliding mode control for under-actuated cranes," *Hierarchical Sliding Mode Control for Under-actuated Cranes*, 2015, doi: 10.1007/978-3-662-48417-3.

[21] H. D. Le and T. Nestorović, "A novel hierarchical recursive nonsingular terminal sliding mode control for inverted pendulum," *Actuators*, vol. 12, no. 12, p. 462, Dec. 2023, doi: 10.3390/act12120462.

[22] Y. Zou, "Nonlinear robust adaptive hierarchical sliding mode control approach for quadrotors," *International Journal of Robust and Nonlinear Control*, vol. 27, no. 6, pp. 925–941, Apr. 2017, doi: 10.1002/rnc.3607.

[23] K. Rsetam, Z. Cao, and Z. Man, "Hierarchical sliding mode control applied to a single-link flexible joint robot manipulator," in *International Conference on Advanced Mechatronic Systems, ICAMechS*, Nov. 2016, vol. 0, pp. 476–481, doi: 10.1109/ICAMechS.2016.7813495.

[24] C. L. Hwang, C. C. Yang, and J. Y. Hung, "Path tracking of an autonomous ground vehicle with different payloads by hierarchical improved fuzzy dynamic sliding-mode control," *IEEE Transactions on Fuzzy Systems*, vol. 26, no. 2, pp. 899–914, Apr. 2018, doi: 10.1109/TFUZZ.2017.2698370.

[25] H. M. Wu and M. Karkoub, "Hierarchical fuzzy sliding-mode adaptive control for the trajectory tracking of differential-driven mobile robots," *International Journal of Fuzzy Systems*, vol. 21, no. 1, pp. 33–49, Feb. 2019, doi: 10.1007/s40815-018-0531-2.

[26] P. T. H. Sen, N. Q. Minh, D. T. T. Anh, and P. X. Minh, "A new tracking control algorithm for a wheeled mobile robot based on backstepping and hierarchical sliding mode techniques," in *2019 1st International Symposium on Instrumentation, Control, Artificial Intelligence, and Robotics, ICA-SYMP 2019*, Jan. 2019, pp. 25–28, doi: 10.1109/ICA-SYMP.2019.8646288.

[27] S. T. Dang, X. M. Dinh, T. D. Kim, H. L. Xuan, and M. H. Ha, "Adaptive backstepping hierarchical sliding mode control for 3-wheeled mobile robots based on RBF neural networks," *Electronics (Switzerland)*, vol. 12, no. 11, p. 2345, May 2023, doi: 10.3390/electronics12112345.

[28] T. Li, X. Liu, and H. Yu, "Backstepping nonsingular terminal sliding mode control for PMSM with finite-time disturbance observer," *IEEE Access*, vol. 9, pp. 135496–135507, 2021, doi: 10.1109/ACCESS.2021.3117363.

[29] H. Razmi and S. Afshinfar, "Neural network-based adaptive sliding mode control design for position and attitude control of a quadrotor UAV," *Aerospace Science and Technology*, vol. 91, pp. 12–27, Aug. 2019, doi: 10.1016/j.ast.2019.04.055.

[30] L. F. C. Ccari and P. R. Yanyachi, "A novel neural network-based robust adaptive formation control for cooperative transport of a payload using two underactuated quadcopters," *IEEE Access*, vol. 11, pp. 36015–36028, 2023, doi: 10.1109/ACCESS.2023.3265957.

[31]   N. N. Zhao, L. B. Wu, X. Y. Ouyang, Y. Yan, and R. Y. Zhang, "Finite-time adaptive fuzzy tracking control for nonlinear systems with disturbances and dead-zone nonlinearities," *Applied Mathematics and Computation*, vol. 362, p. 124494, Dec. 2019, doi: 10.1016/j.amc.2019.06.008.

[32]   W. Lv and F. Wang, "Finite-time adaptive fuzzy tracking control for a class of nonlinear systems with unknown hysteresis," *International Journal of Fuzzy Systems*, vol. 20, no. 3, pp. 782–790, Mar. 2018, doi: 10.1007/s40815-017-0381-3.

BIOGRAPHIES OF AUTHORS

Jose Carlos Vizarreta Mamani ⓘ 🖾 🆂🅲 ↻ was born in Arequipa, Peru, in 2000. He finished his studies in electronic engineering at the National University of San Agustín de Arequipa (UNSA) in 2022. He has specialized in Instrumentation, Automation, and Process Control. He designed the proposed control system, proposed the methodology and wrote the article. He can be contacted at email: jvizarretam@unsa.edu.pe.

Bladimir Leonel Vera Huamani ⓘ 🖾 🆂🅲 ↻ received the B.Sc. degree in electronic engineering from Universidad Nacional de San Agustín de Arequipa, Peru, in 2022. His research interests include control systems and instrumentation. Designed the proposed control system, performed the conceptualization and wrote the article. He can be contacted at email: bverahu@unsa.edu.pe.

Raul Sulla Torres ⓘ 🖾 🆂🅲 ↻ obtained his Ph.D. degree in 2013, he also has a Master of Science in Electronic Engineering mention in Automation and Instrumentation, as well as a Second Specialty in Telecommunications Engineering. He is an Electronic Engineer and is a professor at the National University of San Agustin in Arequipa-Peru. He is currently President of the Chapter of Electronic Engineers of the College of Engineers CD Arequipa, period 2022 to 2024. He was also President of the same Chapter period 2016 to 2018. His areas of interest include automatic control and biomedical engineering. He can be contacted at email: rsullat@unsa.edu.pe.